Fully Automatic Danger Zone Determination for SBRT in NSCLC

Research Article

Tobias Fechter [1] [*], Jose Dolz [2] Alin Chirindel [1,3,4] Matthias Schlachter [4] Montserrat Carles [1] Sonja Adebahr [1,3,4] Michael Mix [6] Ursula Nestle [1]

1 Department of Radiation Oncology, University Medical Center, Freiburg, Germany

2 Inserm U703, Université Lille 2, CHRU Lille, 59120 Loos, France

3 German Cancer Research Center (DKFZ), Heidelberg, Germany

4 German Cancer Consortium (DKTK), partner site Freiburg, Germany

5 VRVis, Vienna, Austria

6 Department of Nuclear Medicine, University Medical Center, Freiburg, Germany

Abstract: Lung cancer is the major cause of cancer death worldwide. The most common form of lung cancer is non-small cell lung cancer (NSCLC). Stereotactic body radiation therapy (SBRT) has emerged as a good alternative to surgery in patients with peripheral stage I NSCLC, demonstrating favorable tumor control and low toxicity. Due to spatial relationship to several critical organs at risk, SBRT of centrally located lesions is associated with more severe toxicity and requires modification in dose application and fractionation, which is currently evaluated in clinical trials. Therefore a classification of lung tumors into central or peripheral is required. In this work we present a novel, highly versatile, multimodality tool for tumor classification which requires no user interaction. Furthermore the tool can automatically segment the trachea, proximal bronchial tree, mediastinum, gross target volume and internal target volume. The proposed work is evaluated on 19 cases with different image modalities assessing segmentation quality as well as classification accuracy. Experiments showed a good segmentation quality and a classification accuracy of 95%. These results suggest the use of the proposed tool may facilitate and speed up the work of clinicians in clinical trials.

1.   Introduction

Lung cancer is the number one cause of cancer death worldwide [1]. The main primary types are small- cell lung cancer and non-small cell lung cancer (NSCLC), whereas around 80% of all cases are NSCLC. High rates of cure

---

* *E-mail: tobias.fechter@uniklinik-freiburg.de*

can be achieved in localized tumors without lymph node metastases (Stage I/II) by surgery. However, due to co-morbidities like chronic obstructive pulmonary disease, high blood pressure or diabetes, about one quarter of all patients is inoperable. For these cases stereotactic body radiation therapy (SBRT) proved to be a good alternative in patients with stage I NSCLC [2–4]. SBRT aims to deliver the prescribed dose in one single or a few fractionated treatment sessions. This involves the irradiation of the tumor with very high doses per session and carries the risk of severe toxicity to the surrounding organs, so called organs at risk (OAR). As a consequence, a very high accuracy in contouring and determining the tumor position during treatment is essential. Dose application and fractionation have to be carefully adapted in these cases, and are currently evaluated within clinical trials against efficacy and toxicity. Central lung tumors are defined as having a distance smaller than a given value from the trachea, the proximal bronchial tree (PROXBT) and the mediastinum (possible values are 20mm for trachea and PROXBT and 5mm for the mediastinum [5]). This area is called the danger zone as it indicates whether a tumor is too close to important organs, and high dose irradiation may cause severe toxicity. With recent improvements in technology and radiation techniques, the treatment has become more precise and the application of SBRT to central lung tumors is currently reconsidered in clinical studies [6] using less aggressive fractionation regimens.

One tool to realize higher precision needed for SBRT is 4D imaging. 3D PET or 3D CT often show a very blurred image of the tumor due to its motion during respiration. 4D imaging depicts the tumor much clearer as the respiratory cycle is divided into several parts (time bins) which allows a better assessment of the tumor shape and size and its motion during breathing. Furthermore the additional usage of PET allows a more accurate delineation of the tumor as it sometimes shows parts of the tumor that occur on the CT as normal tissue. Several methods exist to delineate the tumor in 4D [7].

In this work we use the internal target volume (ITV) approach with the 4D PET which means that we delineate the gross target volumes (GTV) in the 3D time bins of the 4D PET and combine them to the ITV to cover the full extent of the tumor.

The discrimination whether a tumor is central or peripheral in the clinic is done visually by a physician. Currently used software in clinical practice offer 2D slice by slice display of the image data-sets which makes it difficult to precisely measure 3D distance from the tumor to the surrounding organs. To our knowledge at the moment, no tools exist to automatically detect the danger zone around mediastinum, PROXBT and trachea and to discriminate central and peripheral tumors. However, there are dedicated approaches for mediastinum, trachea and PROXBT as well as PET GTV segmentation.

Segmenting the mediastinum is a difficult task, as it is a very heterogeneous structure with vague boundaries.

Few works exist that dealt with mediastinum segmentation directly [8, 9]. Both segment the mediastinum by finding the borders of the mediastinum and connecting them with a shortest path algorithm. For the following reasons, neither approach satisfies our needs:

- The vertebral body as well as the mediastinal structures should be subject to the lowest possible radiation dose, therefore both, mediastinum and vertebral bodies are encompassed by the danger zone. Current approaches treat mediastinum and vertebral body segmentation separately. In this work, vertebral body segmentation is included into mediastinum delineation because of the contextual correlation and the spatial adjacency. Hereinafter the term mediastinum segmentation encompasses the delineation of the mediastinum and the vertebral body.

- The datasets at hand consist of chest CT as well as full body CT, both with and without contrast agent. There are significantly different image properties between contrast enhanced CT and low dose non-contrast CT.

- A proper mediastinum delineation demands a determination of the diaphragm, which represents the caudal border of the mediastinum and was neglected in previous works.

The basis of the mediastinal segmentation approach outlined in this work, is similar to both methods mentioned above [8, 9], with the differences that it detects the diaphragm, can deal with multiple modalities and segments the vertebral body together with the mediastinum. The organs segmented to determine the mediastinum are: body, lungs, bony structures, diaphragm, spinal canal and sternum. Although, these contours used for mediastinum detection are not as detailed as dedicated methods, they can be used as a good starting point for advanced organs at risk segmentation.

There has been a lot of work done on the topic of trachea and PROXBT segmentation. Approaches include methods such as region growing [10, 11], mathematical morphology [12], energy minimization [13] and rule based [14] techniques. All of them are highly specialized and segment the bronchial tree to a detailed extent. Segmentation up to the second or third bifurcation is fully sufficient for the purpose of the presented work. Therefore we combined some basic image processing algorithms to achieve a fast segmentation with the required level of detail.

The range of PET GTV delineation algorithms is very wide [15]. These algorithms make use of a variety of image segmentation methods like: edge detection, thresholding, region growing, clustering, stochastic models, deformable models, machine learning. Most of the proposed methods were developed for 3D data-sets. For segmenting 4D data-sets, an algorithm that handles big data in a short amount of time is needed. In this work we use a 4D threshold and region-growing based algorithm [16], which has proven to be fast and accurate.

Here we present a highly versatile tool able to fully automated segment trachea, PROXBT, mediastinum, GTV and ITV and which can handle chest CT, full body CT, both with and without contrast agent, 18 FDG-PET and 4D 18 FDG-PET. The segmentations are used to determine the danger zone around the mediastinum, the vertebral body, the PROXBT and the trachea. Then the overlap of the danger zone with the GTV or ITV respectively is calculated. If there is an overlap the tumor was classified as central, otherwise as peripheral. This tool was implemented into the medical imaging toolkit (MITK) framework [17] and gives user feedback via a graphical user interface about the outcome of the calculations. The proposed tool can be used in the clinic to automatically classify patients for conventional treatment and SBRT or to automatically determine patients suitable for a clinical trial of SBRT on central NSCLC.

2. Materials & Methods

2.1. Segmentation and Danger Zone Determination

For segmentation a top down approach similar to the mediastinum segmentations [8, 9] is used. Firstly, large and clear structures are delineated by the algorithm. The results are then used for more sophisticated delineations. By using this method, procedures in a later step can make use of knowledge gained in a previous step. Thereby, even the segmentation of difficult structures is manageable with basic image processing algorithms. An abstract depiction of this procedure is given in Fig. 1. In this section different steps of the algorithm are outlined in the same order as they are applied in the segmentation procedure. To get the mediastinum, trachea, PROXBT, GTV and ITV segmentations some intermediate steps have to be done. First, the body is segmented, followed by the delineation of bony structures, lungs, PROXBT and trachea, which make use of the previous body segmentation. The spinal canal is detected by using the bone and lung segmentation, the diaphragm segmentation makes use of the lung segmentation and the sternum takes bone, spinal canal and lung as input. With sternum, lung and diaphragm the mediastinum is outlined and used together with the trachea and the PROXBT to determine the danger zone. For the tumor segmentation, lung as well as mediastinum serves as input.

2.1.1. Body

The body segmentation is done on the CT. First a threshold is determined by iterating along one diagonal of the center slice and searching for the largest intensity difference of two successive pixels. This corresponds with the transition from air to tissue in the image. The pixel intensities of the two pixels with the largest intensity difference are $I(v_1)$ and $I(v_2)$, respectively. The threshold is calculated as the average intensity of $I(v_1)$ and $I(v_2)$.

The threshold is applied to the CT and the largest connected region is extracted. This process is followed by a hole filling algorithm to include again structures inside the body that were eliminated by the threshold.
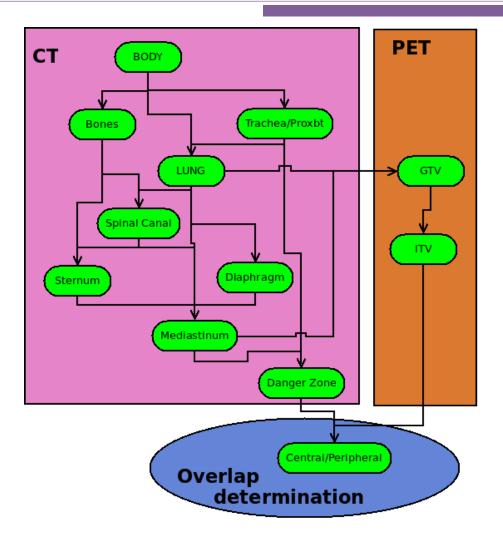
Figure 1: A schematic presentation of the segmentation work flow. The green shapes show the performed steps, the boxes indicate on which modality this step is processed and the arrows represent the transfer of information from one step to another. In the blue ellipse the division in central or peripheral tumor is done by calculating the overlap of ITV and danger zone. The whole process starts with the body segmentation step.

Eventually 3D and 2D morphological operators are applied to remove the table and the fixation. The 3D operator has a radius of 2 voxels, the 2D operator a radius of 3 pixels. The operators are applied in the following order: 3D erosion, 2D slice-wise erosion, 2D slice-wise dilation, 3D dilation. After 3D erosion only the largest connected region is kept, after 2D erosion every region with an area smaller 3900 mm^2 is deleted. The value of 3900 mm^2 proved to be high enough to remove all unwanted structures and low enough to keep smaller body parts like arms. An example of the extracted body can be seen in image in Table 1a.
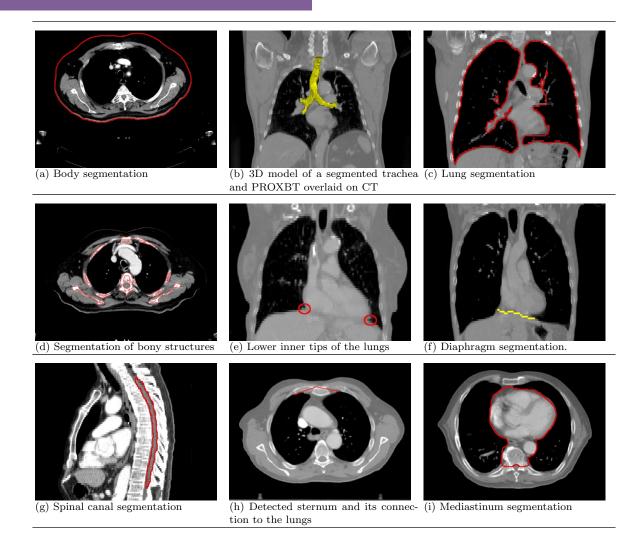
(a) Body segmentation

(b) 3D model of a segmented trachea and PROXBT overlaid on CT

(c) Lung segmentation

(d) Segmentation of bony structures

(e) Lower inner tips of the lungs

(f) Diaphragm segmentation.

(g) Spinal canal segmentation

(h) Detected sternum and its connection to the lungs

(i) Mediastinum segmentation

Table 1: Structures segmented in the work flow of the presented algorithm.

2.1.2. Trachea and PROXBT

The trachea and PROXBT are segmented in 2 steps. First, an iterative threshold method is applied and then an analysis step is performed to remove unnecessary structures from the segmentation.

The first step starts by applying an initial threshold range of -1024 to -600 Hounsfield Units (HU) to the CT masked with the body segmentation to get the air containing structures. The resulting binary image is eroded with a 2D disk of one pixel radius along the axial plane. The two largest connected regions after erosion are assumed to be part of the lungs. The tips of the lungs are then determined and the slice 15mm above the upper tip is set to be the slice to start looking for the trachea. From the starting slice downward the first region with an area of 40mm^2 on the eroded binary image is searched. Taking into account that the lower border for the

diameter of the human trachea is around 10 mm [18], that the trachea is not a perfect circle as well as the preceding erosion a threshold of 40mm^2 proved to be appropriate. From this area a region growing is started downwards. The obtained region is then dilated with the above mentioned disk. If the smallest possible bounding box containing the resulting volume is smaller than a third of the body diameter in transverse direction and half of the body diameter in longitudinal direction, the algorithm terminates and the volume is set as trachea and PROXBT segmentation. Otherwise the upper threshold is decremented by 50 HU and the algorithm starts again. The comparison of the bounding box with the body diameter is done to be sure that the region growing algorithm did not grow into the lungs.

In the second step the segmentation result of step one is subdivided into multiple parts by splitting the volume at the bifurcations. Then all parts with a length lower than 1cm are deleted from the segmentation.

The value of 1cm was specified by a clinician, all parts smaller go too deep into the lungs and would cause an overlap of peripheral tumors with the danger zone. A 3D model of a segmented trachea can be seen in the image in Table 1b.

2.1.3. Lungs

The lungs are segmented by applying first the final threshold range obtained in subsection II-A2 to the CT masked with the body segmentation. Then the largest connected area is extracted, which yields left and right lung plus trachea and PROXBT. To get the lungs, the trachea and PROXBT (segmented in II-A2) binary volumes are subtracted. As a final step a closing filter is applied to eliminate holes in the lungs due to denser tissue. A segmentation example can be seen in the image in Table 1c.

2.1.4. Bony Structures

The bony structures in the CT image are segmented by using a threshold range from 200 to 3500 HU. As in all previous steps the CT is again masked with the body segmentation. To get rid of false positive segmented areas like calcifications, all segmented structures with a volume lower than 1100 mm^3 are removed. The volumes left belong to the ribs, the sternum, the vertebra, long continuous calcifications on the aortic wall as well as contrast agent in the case of contrast enhanced CT. A segmentation example of the bony structures can be seen in the image in Table 1d.

2.1.5. Diaphragm

The diaphragm or thoracic diaphragm is a thin muscle that separates the thoracic cavity from the abdominal cavity. In this work the diaphragm is used as lower border for the mediastinum segmentation. Therefore, only

the part adjacent to the mediastinum is of interest for the algorithm. The part of the diaphragm left and right to the mediastinum is directly connected to the lungs and the ribs. For this reason the diaphragm segmentation takes the lung segmentation of step II-A3 as starting point.

First, the binary image representation of the lung segmentation is converted to a surface by applying a marching cube algorithm [19]. Then the normals of the surface are calculated and the two largest areas with normals along the caudal direction $\pm$ 20 degree are determined. These two areas correspond to the bottom of the lungs. In the next step, for every coronal slice the inner tips of the lung bottom areas are detected (encircled in the image in Table 1e). To retrieve the part of the diaphragm between the lungs for every coronal slice the two inner tips of the lung bottoms are connected. Connections are done by using the shortest path (minimal edge sum) algorithm by Dijkstra [20]. To do this, the axial slices are transformed into graphs with a vertex v for every pixel and an edge e connecting vertices representing adjacent pixels. The edge weight w_{ij} for e_{ij} connecting v_i and v_j is calculated with:

$$w_{ij} = (I(v_i) - I(v_j))^2 + \frac{angle(\nabla I(v_i), \nabla I(v_j))}{\pi} * 1000 + I(v_j)^2 \tag{1}$$

where $I(v_i)$ represents the intensity of the pixel represented by v_i, ∇ is the gradient, angle gives the angle in radians, $w_{ij} \in R$ and $v_i \in R_3$. The first two parts of equation 2 penalize different intensities and gradients, while the third part punishes HU untypical for muscles (usually close to zero). After the slice-wise application of the Dijkstra algorithm the resulted area is smoothed with a mean filter to weaken outliers. An example slice of a diaphragm segmentation can be seen in the image in Table 1f.

2.1.6. Spinal Canal

The spinal canal is a tubular structure in the spine through which the spinal cord passes. The spinal canal serves as the posterior border for the mediastinum segmentation. First, the most posterior parts of the spine along the height of the lungs are determined. Then, an elliptical structuring element (SE) is aligned to detect the canal.

To detect the posterior tips of the spine a search area is defined. The search area spans from the center of mass of the lung segmentation done in step II-A3 to the posterior end of the image in the sagittal axis, from the cranial to the caudal end of the lung along the longitudinal axis and with a width of 4cm in lateral direction. In this search area the most posterior bony structure (already segmented in step II-A4) is determined for every slice. An example of the search area, the center of mass and the determined spine tip can be seen in Fig. 2.

The diameters for the elliptical SE for the canal detection are 9mm in the sagittal and the transverse axis and 21mm in the longitudinal axis. The SE is applied to every slice that contains a part of the lungs. The starting point for every slice is the mean position of all spine tips $\pm$ 10mm from the current slice. The SE is then moved in a 53 degree funnel anterior until it encompasses a volume without bony structures. A funnel with an angle of

53 degree is wide enough to cover the spinal canal plus offering a small buffer to be invariant to small rotations (Fig. 2). In the last step outliers are eliminated and the result is smoothed. A segmentation example is shown in the image in Table 1g.
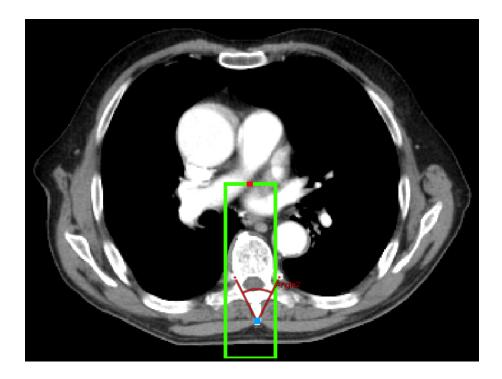

Figure 2: The green rectangle marks the search area for the posterior tip of the spine. The red square indicates the center of mass of the lungs and the blue square shows the found posterior tip of the spine. The red angle represents the search funnel for the spinal canal.

2.1.7. Sternum

The sternum is a bony structure opposite to the spinal canal. It serves as anterior border for the mediastinum segmentation used in this work. For this purpose it is sufficient to find only one pixel per slice that belongs to the sternum. For every slice that contains a part of the spinal canal segmentation a ray tracing algorithm [21] is applied with the canal center as starting point for the rays. The rays are shot in anterior direction ± 5 degrees with a step size of 1 degree. The step size along the ray is one pixel. The sternum pixel is determined by finding the bony structure with the biggest distance to the spinal canal in anterior direction on the ray with the lowest angle.

To get a continuous anterior border for the mediastinum segmentation the sternum pixels are connected to the lungs. This is again done with a slice-wise ray tracing. The starting points for the rays are the determined

sternum pixels. The rays are first shot in both lateral directions, then the angle to the posterior direction is decreased until a lung point is hit. The hit lung point is then connected to the sternum pixel with a straight line. An example can be seen in the image in Table 1h.

2.1.8. Mediastinum

The mediastinum is a volume containing a lot of different structures such as heart, aorta, parts of the trachea, esophagus etc. Segmenting these structures individually is a difficult task, because of the different appearance on CT. The proposed approach uses the structures that bound the mediastinum to apply an adaptive iterative region growing method that filled the volume in-between. In particular, these bounds are the lungs (II-A3) in transverse direction, the sternum (II-A7) in anterior, the spinal canal (II-A6) in posterior and the diaphragm (II-A5) in caudal direction. As this work deals only with lung tumors the cranial border is the area spanned by the two cranial lung tips.

In a pre-processing step, edges on the CT image are determined in all slices that cover lung tissue by applying a Laplacian-of-Gaussian [22] followed by a zero-crossing detection. The region growing is done with an elliptical SE of varying size. If the SE does not overlay with a "disturbing structure" the center pixel of the SE will be included into the mediastinum segmentation. The growing process can be divided into three steps: initialization, rough growing and fine growing.

In the initialization step the diameters of the elliptical sized SE are set to 18mm in sagittal, 14.4mm in transverse and 8.4mm in longitudinal axis. The starting point for the region growing is found by centering the SE on the center of mass of the lungs. If the SE overlaps with the lungs in this position, it is moved in sagittal, transverse and longitudinal direction until there is no overlap.

In the rough growing step the region grows until the SE overlaps with a "disturbing structure". The "disturbing structures" in this step are lungs, diaphragm, spinal canal and the sternum and its connection to the lungs. This step is done to roughly cover all structures in the mediastinum but not to grow out of the mediastinum (e.g. into an adjacent tumor or vessels going into the lungs).

In the fine growing step diameters are set to 3.5mm in sagittal and transverse axis and 2.5 in longitudinal axis. The starting points are the border points of the last region growing step. In this step also the edges detected in the pre-processing are added to the "disturbing structures". This makes sure that the SE fills only structures that were already partly covered by a previous step and does not grow out of the mediastinum. An example where the tumor is connected to the mediastinum but the region growing did not include it to the segmentation is show in Fig. 3.

After every region growing step the particular result is dilated with the size of the SE to include also the pixels between the center of the SE and the border. A final result of a segmented mediastinum can be seen in the image in Table 1i.

Figure 3: The green circle marks a tumor. The fine region growing step combined with the edge detection makes sure that the tumor is not included into the mediastinum segmentation (red line) although they are connected and have tissue with similar HU.

2.1.9. Tumour

The tumor segmentation is done on ^{18}FDG-PET data-sets as the tumor is more clearly distinguishable from healthy tissue in this modality. The problem with segmenting PET images automatically is that also healthy tissue (e.g. heart) shows a high tracer accumulation in a large number of cases, which makes it hard to differentiate it from tumor as PET offers no anatomical information. To exclude these structures the algorithm makes use of the existing registration of PET and CT. During CT acquisition the patient holds its breath after inhalation to depict the fully unfolded lung. The lung mask done on this CT is either as big as (inhale time bin in a 4D PET) or bigger (ungated PET, exhale time bin in a 4D PET) than the lung seen on PET. The presented approach assumes that the registration between CT and PET is correct. Therefore one has to be aware that there is still a small chance that the algorithm misses a small extreme peripheral lung lesion obscured by registration errors.

The algorithm used for segmentation [16] consists of 2 steps. A thresholding and a region growing step. The thresholding step is applied on the PET image masked with the lungs segmentation done on CT. But for the region growing, the unmasked image is used to allow the segmentation of tumors grown out of the lungs. The algorithm yields either a 3D or 4D GTV, depending on the dataset at hand and an ITV. A 4D GTV consists of at least 2 3D GTVs. In 3D cases the ITV and the GTV are the same.

In some cases, parts of the heart with high tracer accumulation overlap with the lungs segmented on CT. An example can be seen in Fig. 4. Therefore, some additional knowledge was incorporated. A delineated volume by the tumor segmentation algorithm has to fulfill the following properties to be accepted as tumor volume:

- the volume has to be at least 320 mm^3

- the volume has to be lower than 37 cm^3

- at least 10% of the volume has to be inside the lungs.

The volume of 320 mm^3 corresponds to 5 voxels of the PET volume and is to eliminate false positive segmentation due to noise. The volume of 37 cm^3 corresponds roughly to the volume of the left ventricle and is to eliminate a segmentation of the heart if the lung masking does not exclude the heart's high uptake perfectly. For 4D data-sets the above mentioned points are only evaluated for the first time bin.

2.1.10. Danger zone

The danger zone is created by adding a 2cm margin to the trachea and the PROXBT and a margin of 0.5cm to the mediastinum. Afterwards the area of the tumor overlapping with the danger zone is calculated by a logical AND operator. An example of the danger zone and a segmented overlapping tumor is shown in Fig. 5.

2.2. Data-sets and Evaluation

Nineteen patient cases were used to evaluate the presented work. We included 13 Patients with primary or relapsed NSCLC (UICC stage: n=10, II: n=2, III: n=1) and 6 patients with solitary metastases of NSCLC, head and neck or colorectal cancer. All had one CT and one 18 FDG-PET both registered to each other. Eighteen patients had a full body CT and 1 had a chest CT (Fig. 6c). The chest CT and 10 full body CTs (Fig. 6d) were without contrast agent, the remaining 8 showed contrast agent (Fig. 6e). 15 Patients had a 4D PET with 10 bins (Fig. 6a), 3 a full body PET (Fig. 6f) and 1 a 3D PET showing only the chest (Fig. 6b). A detailed overview of the properties of the dataset types is given in Table 2.
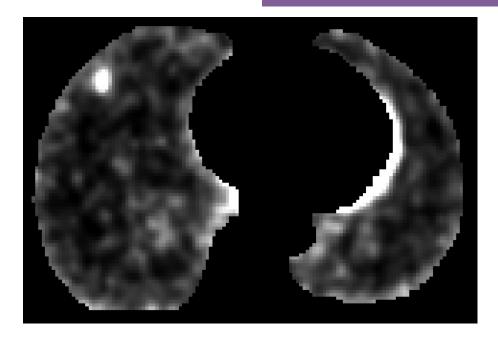
Figure 4: The PET masked with the segmentation of the lungs on CT. The high tracer accumulation in the heart cannot be fully removed by the masking because of different resolutions and a mismatch of the tracer uptake in PET and anatomy seen on CT.

Data-set type	Resolution	Voxel size (mm)
full body CT	512x512x(192-255)x1	(1.17-1.37)x(1.17-1.37)x4.00
chest CT	512x512x90x1	1.17x1.17x2.00
full body PET	320x416x213	1.80x1.80x4.00
chest PET	(288-320)x(288-416)x89x1	(1.80-2.00)x(1.80-2.00)x2.00
4D PET	144x144x45x10	4.00x4.00x4.00

Table 2: Resolution and voxel size of all dataset types used in this work. When different values occurred within one dataset type only the range is shown in the table.

All cases were classified by an experienced clinician to have either a peripheral (9 cases) or a central tumor (10 cases). The clinician used the same parameters (distance of tumor to mediastinum, trachea and PROXBT) for classification as the introduced algorithm. This classification served as ground truth for the evaluation of this work. For the evaluation, the classification of the 19 patients by the presented algorithm was compared to the classification of the clinician.

Trachea and PROXBT segmentation, including all steps necessary for it, as well as the tumor segmentation algorithm were evaluated in previous work [23] [24]. The mediastinum contours were assessed visually by an experienced clinician by using an adapted version of the alignment score [25]. With this method the expert rates each contour with a number from 1 to 5. The meaning of the numbers is given in Table III. The results are
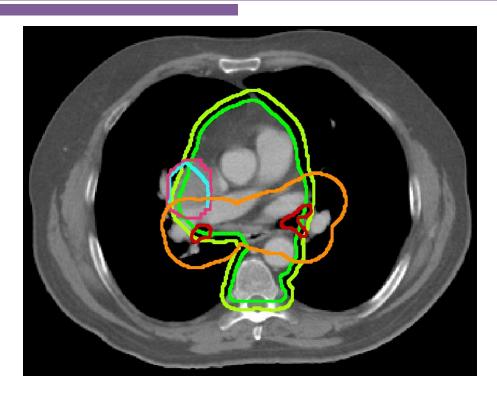
Figure 5: In this picture mediastinum, trachea and PROXBT, GTV, ITV and danger zone segmentation results can be seen. The red line stands for trachea and PROXBT, the green one for the mediastinum, the cyan indicates one GTV and the pink is the ITV containing all GTVs. The danger zone is depicted with yellow (around mediastinum) and orange (around trachea and PROXBT). An overlap of the tumor with all structures but the trachea and PROXBT can be clearly seen.

shown in Section III. Spinal canal, sternum, lungs and diaphragm were not separately evaluated as they are only used as input for the determination of the mediastinum.

The computations were done on a 64 bit machine with an Intel Core i5-2400 3.40 GHz processor and 4 GB RAM. The graphics card was not used for computations.

score	meaning
1	not usable
2	poor
3	average
4	good
5	excellent

Table 3: The score and its meaning used for the rating of the mediastinum contour.
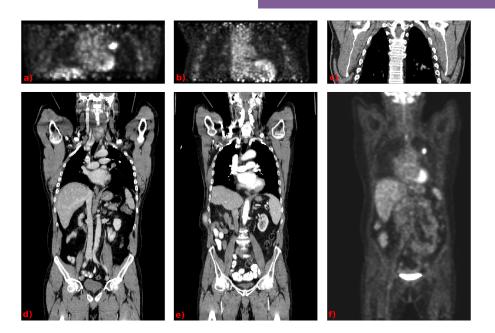
Figure 6: Example slices of the dataset types used (a: 4D PET, b: chest PET, c: chest CT, d: full body CT, e: full body CT with contrast agent, f: full body PET). CT depicts clearly the anatomical structure of the human body, whereas scans with contrast agent show organs in a different way than scans without contrast agent. PET is capable to depict biochemical and physiological processes. Bright structures indicate high tracer accumulation. In the case of [18]FDG-PET the tracer accumulates in areas with high glucose metabolism (e.g. heart, brain and tumor).

2.3. Implementation

For making the whole framework accessible for clinicians, the algorithm was implemented as a plug-in in the free open source software framework MITK. MITK offers user dialogs to load the appropriate data. After loading the data the user has to click the start-button to start the algorithm. Once all calculations are done the plug-in indicates by two colored areas whether there is an overlap of the tumor with the danger zone or the organs. Initially, color areas are filled in gray color. The first color area will become red or green, regarding whether there is an overlap with the danger zone or not, respectively. The second color area will define the existence of overlap with the mediastinum, trachea or PROXBT. As in the first color area, red indicates overlap, whereas green means no overlap. If the user wants bigger or smaller margins for the danger zone determination he or she can change them with input fields and the results will be updated in real time. A screen-shot of the graphical user interface can be seen in Fig. 7.
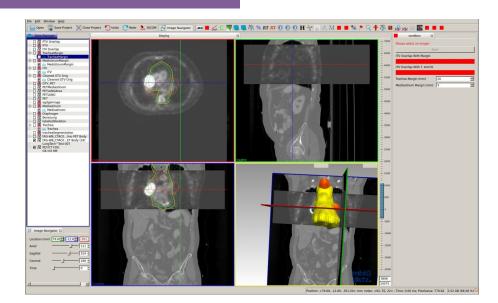
Figure 7: A screen-shot of the implementation of the algorithm into the MITK framework. The user can load data-sets with the MITK internal dialogs, and start the algorithm with the start button of the plug-in. The result is then indicated with two color areas in the plug-in (red for overlap, green for no overlap). Furthermore the user can change the margins with the input fields below the color areas, and the results will be updated in real time.

3. Results

The rating of the mediastinum segmentations by an expert yielded an average score of 4.37, which translates between good and excellent on the grading scale. 12 contours were rated with score 4 and 7 contours with score 5. An overview of all cases is depicted in Fig. 8 (peripheral) and Fig. 9 (central).

The presented algorithm classified 18 of 19 cases correctly. Only in 1 case (Fig. 10) the algorithm did not agree with the opinion of the clinician. Fig. 10a shows the tumor depicted by CT, Fig. 10b depicted by PET. The clinician classified the tumor as central whereas the proposed algorithm classified the tumor as peripheral. The CT demonstrates that that the tumor is connected to the left hilum and therefore appears to overlap the danger zone. On PET, on the other hand the tumor looks like a typical peripheral tumor. In this case the clinician based the decision more on the information offered by the CT than the one offered by PET. After the testing phase the result of the algorithm was shown to the clinician, who reconsidered the decision based on the algorithm result and reclassified the tumor as peripheral. This improved the classification accuracy of the algorithm to 100%.

In one case the trachea segmentation failed because of a narrowing in the upper part. The narrowing, shown in Fig. 11, made the trachea and PROXBT segmentation fail. After the erosion explained in subsection II-A2 the

applied region growing algorithm was not able to pass this passage. The usage of more knowledge about the anatomy of the trachea by the algorithm may solve this problem. For instance, by allowing the region growing to skip a slice to bridge a constriction if the segmented volume is too small or a given bifurcation is not reached yet. Nevertheless, the case was classified correctly as central tumor.
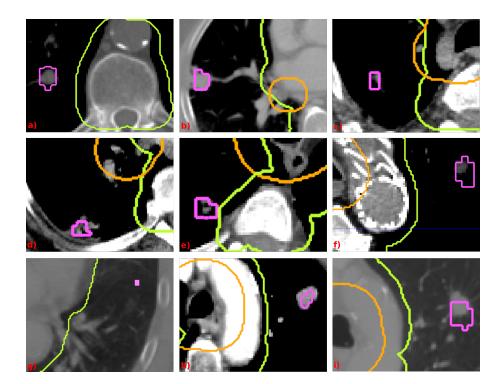

Figure 8: All cases classified as peripheral by the clinician. The figure shows the PET GTV (pink), the mediastinum and vertebral body margin (green) and the trachea and PROXBT margin (orange) segmented by the algorithm.

In another case, false positive tumor spots were segmented. This was due to a common problem in PET image segmentation in which false positive tumor delineation is a result of increased tracer accumulation, which can sometimes surpass the tracer uptake within the tumor. In Fig. 12 the tumor encircled in green shows a lower uptake than the areas outlined in red. This problem is similar to the one shown in Fig. 4. Also the masking of the tumor with the lungs did not solve the problem because parts of the tracer uptake of healthy tissue were still visible inside the lung. Here, a segmentation of the tumor on both PET and CT can probably increase the accuracy of the tumor segmentation. However, in this case, it had no impact on the classification result, because the spots were located at the most outer parts of the lungs. The mean computation time was about $3\frac{1}{2}$ minutes per case.
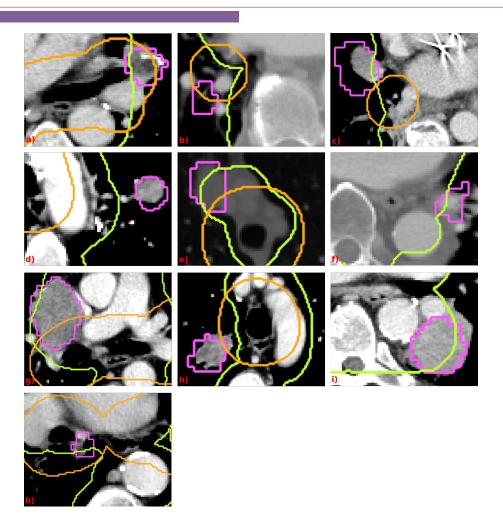
Figure 9: All cases classified as central by the clinician. The figure shows the PET GTV (pink), the mediastinum and vertebral body margin (green) and the trachea and PROXBT margin (orange) segmented by the algorithm.

Twelve mediastinal contours were classified good and not as excellent. The main reason for this was that the segmentation algorithm missed either some parts of the lower part of the heart or of the upper part of the mediastinum. The false negative segmentation of the lower heart was due to an erroneous diaphragm segmentation which yielded incorrect borders for the region growing algorithm. An extreme example can be seen in Fig. 13a. In this case an over-sized heart pushed the left lung in cranial direction, which caused the diaphragm segmentation to draw the border between thoracic and abdominal boundary above the heart. Nevertheless the segmentation was sufficient for the algorithm as only the region of the mediastinum between the lungs is needed for an accurate computation. The missed parts of the mediastinum in the upper area were due to a small diameter of the mediastinum that the larger SE was not able to pass. Therefore the smaller SE segmented only the parts that were connected to lower structures already segmented with no edge in between. This yielded a
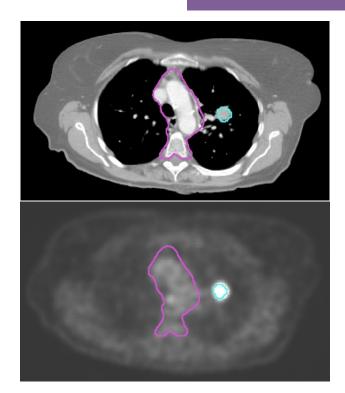
Figure 10: A tumor classified central (GTV in cyan) by the clinician and peripheral by the proposed algorithm. On CT (10a - top) the tumor seems to be connected to the mediastinum (pink) whereas on PET (10b - bottom) the tumor occurs peripheral. After showing the clinician the algorithm result, the clinician reconsidered the decision and reclassified the tumor as peripheral.

spotted segmentation which can be seen in Fig. 13b.

4. Discussion

The differentiation of central and peripheral lesions plays a key role in determining the clinical appropriateness of SBRT and is important for treatment planning. The use of the presented work facilitates this task for clinicians. To our knowledge there exists no tool that discriminates central and peripheral tumors and a segmentation of OARs automatically at the same time. Testing yielded a good segmentation quality and 95% classification accuracy. However, there are still issues to improve to increase performance and accuracy.

One problem with tumor segmenting using PET images is that also healthy tissue (e.g. heart) can show a high tracer accumulation, which makes it hard to differentiate it from tumor as PET offers no anatomical
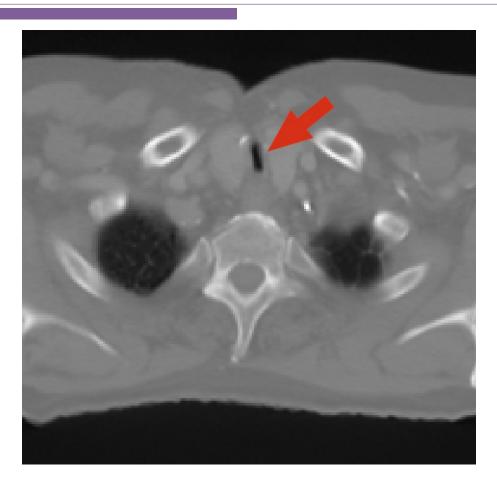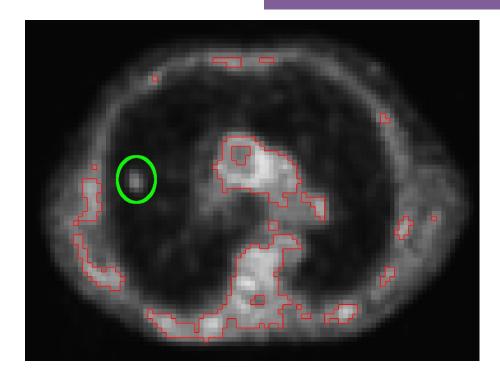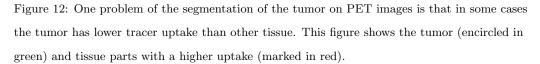
Figure 11: The narrowing of the trachea seen on this CT slice led to an error in the trachea and PROXBT segmentation because the applied region growing algorithm was blocked by this narrow passage.

information. Therefore a delineated volume by the tumor segmentation algorithm has to fulfill additional conditions to be accepted as tumor volume. At least 10% of the potential tumor volume have to be in the lungs. Thus some centrally, within the mediastinum located tumors might not be detectable with the presented algorithm.

The hierarchical architecture enables the use of basic image processing algorithms which are easy to implement. This hierarchical approach has assets and drawbacks. On the one hand an error in an early step may influence the following calculations. In Fig. 1 can be seen that the trachea, PROXBT and lungs segmentation steps are crucial for the following steps. An error in one of these steps, e.g. a failure in the separation of lungs and trachea, affects all following steps and may lead to a wrong result. On the other hand the hierarchical module based design makes the whole algorithm more stable. An error in one step has no influence on parallel steps and the algorithm can still yield a correct result although one step failed (as it was shown in III).

Figure 12: One problem of the segmentation of the tumor on PET images is that in some cases the tumor has lower tracer uptake than other tissue. This figure shows the tumor (encircled in green) and tissue parts with a higher uptake (marked in red).

A source of error that can never be fully eliminated are anatomical variations due to pathological processes or medical interventions. Steps most susceptible to these errors are trachea, lungs and spinal canal segmentation. One surgical intervention that may influence the segmentation of the spinal canal is laminectomy. The removal of the posterior aspect of the vertebral body could lead false starting positions for the SE. However the smoothing over several starting positions should eliminate or reduce the error. Future testing has to prove this concept as no data-sets with a laminectomy where at hand during testing. Pleural effusion is a pathology that can influence the lung segmentation and subsequent steps. Because of fluid that accumulates in the pleural cavity the diaphragm is no longer directly adjacent to the air filled part of the lungs that is segmented by the algorithm. The subsequent diaphragm segmentation step connects the two lungs, which results in a false segmentation cranial to the real diaphragm position. A lesion inside the pleural effusion would be missed as the algorithm is designed for lesions inside or at the border of the air filled part of the lungs. Another issue caused by pleural effusion (or other abnormalities like pneumothorax) may be the fail of separation of trachea and lungs (II-A2) when the volume covered by the trachea exceeds the volume covered by the affected lung.

The presented segmentation approach for the mediastinum delineates mediastinum and vertebral body as one structure although the vertebral body is anatomically not part of the mediastinum. Beyond spinal cord toxicity
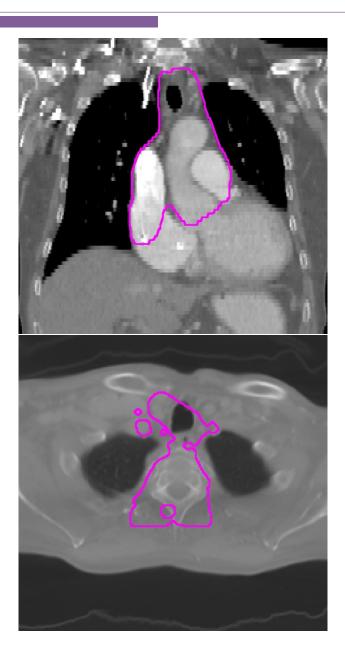
Figure 13: Two examples of mediastinal segmentation errors. In Fig. 13a (top), the heart was missed by the segmentation algorithm because of the small left lung. In Fig. 13b (bottom), the SE was too large for the small part of the mediastinum between the lungs which yielded a spotted segmentation by the smaller SE.

SBRT induced fractions of bony structures are reported in current literature [26], however little is known about the dose/fractionation response of the vertebral body. Due to this uncertainty a conservative approach was chosen and the vertebral body was included into the mediastinum segmentation. In cases with multiple lesions visible on PET, the algorithm would segment all lesions separately and yield different GTVs and ITVs. However,

the classification step and the GUI are designed to classify case-wise. A patient will be classified central if at least one central tumor node is present.

The mediastinum segmentation approach outlined in this work, pre-segments body, lungs, bony structures, diaphragm, spinal canal and sternum before the actual mediastinum detection. These structures may not be as accurate as the results of dedicated methods but they could be used as a good starting point for advanced organs at risk segmentation.

5. Conclusion

In this work a novel, highly versatile, multimodality tool for assistance of NSCLC treatment planning in radiotherapy is presented. The proposed tool classifies NSCLC into peripheral or central without user interaction. Furthermore it segments trachea, PROXBT, mediastinum, GTV and ITV automatically. The testing on 19 cases showed a good segmentation quality and a classification accuracy of 95%. Evaluation revealed the need to improve some steps to get more invariant to anatomical variations. In summary, the proposed tool may facilitate clinical trial data analysis and speed up NSCLC patients treatment planning but further testing and improvements have to be done.

References

[1] B. W. Stewart and C. P. Wild, *World Cancer Report 2014*. World Health Organization, 2014.

[2] Y. Nagata, K. Takayama, Y. Matsuo, Y. Norihisa, T. Mizowaki, T. Sakamoto, M. Sakamoto, M. Mitsumori, K. Shibuya, and N. Araki, "Clinical outcomes of a phase I/II study of 48 Gy of stereotactic body radiotherapy in 4 fractions for primary lung cancer using a stereotactic body frame," *International Journal of Radiation Oncology* Biology* Physics*, vol. 63, no. 5, pp. 1427–1431, 2005.

[3] R. Timmerman, R. Paulus, J. Galvin, J. Michalski, W. Straube, J. Bradley, A. Fakiris, A. Bezjak, G. Videtic, and D. Johnstone, "Stereotactic body radiation therapy for inoperable early stage lung cancer," *JAMA*, vol. 303, no. 11, pp. 1070–1076, 2010.

[4] I. S. Grills, V. S. Mangona, R. Welsh, G. Chmielewski, E. McInerney, S. Martin, J. Wloch, H. Ye, and L. L. Kestin, "Outcomes after stereotactic lung radiotherapy or wedge resection for stage I non–small-cell lung cancer," *Journal of Clinical Oncology*, vol. 28, no. 6, pp. 928–935, 2010.

[5] R. Timmerman, R. McGarry, C. Yiannoutsos, L. Papiez, K. Tudor, J. DeLuca, M. Ewing, R. Abdulrahman, C. DesRosiers, and M. Williams, "Excessive toxicity when treating central tumors in a phase II study of

stereotactic body radiation therapy for medically inoperable early-stage lung cancer," *Journal of Clinical Oncology*, vol. 24, no. 30, pp. 4833–4839, 2006.

[6] European Organisation for Research and Treatment of Cancer – EORTC, "LungTech: Stereotactic body radiotherapy (SBRT) of inoperable centrally located NSCLC - NLM identifier: NCT01795521," *ClinicalTrials.gov [Internet]; NLM, Bethesda MD*, 2000.

[7] J. W. Wolthaus, J.-J. Sonke, M. van Herk, J. S. Belderbos, M. M. Rossi, J. V. Lebesque, and E. M. Damen, "Comparison of different strategies to use four-dimensional computed tomography in treatment planning for lung cancer patients," *International Journal of Radiation Oncology* Biology* Physics*, vol. 70, no. 4, pp. 1229–1238, 2008.

[8] S. L. Volpi, M. Antonelli, B. Lazzerini, F. Marcelloni, and D. C. Stefanescu, "Segmentation and reconstruction of the lung and the mediastinum volumes in CT images," in *Applied Sciences in Biomedical and Communication Technologies, 2009. ISABEL 2009. 2nd International Symposium on*, pp. 1–6, IEEE, 2009.

[9] J. Zhang, Z. He, and X. Huang, "Automatic 3D anatomy-based mediastinum segmentation method in CT images," *International Journal of Digital Content Technology and its Applications*, vol. 5, pp. 266–274, July 2011.

[10] R. Chiplunkar, J. M. Reinhardt, and E. A. Hoffman, "Segmentation and quantitation of the primary human airway tree," in *Medical Imaging 1997*, pp. 403–414, International Society for Optics and Photonics, 1997.

[11] T.-Y. Law and P. Heng, "Automated extraction of bronchus from 3D CT images of lung based on genetic algorithm and 3D region growing," in *Medical Imaging 2000*, pp. 906–916, International Society for Optics and Photonics, 2000.

[12] C. Pisupati, L. Wolff, E. Zerhouni, and W. Mitzner, "Segmentation of 3D pulmonary trees using mathematical morphology," in *Mathematical morphology and its applications to image and signal processing*, pp. 409–416, Springer, 1996.

[13] C. I. Fetita and F. Prêteux, "Quantitative 3D CT bronchography," in *Biomedical Imaging, 2002. Proceedings. 2002 IEEE International Symposium on*, pp. 221–224, IEEE, 2002.

[14] M. Sonka, W. Park, and E. A. Hoffman, "Rule-based detection of intrathoracic airway trees," *Medical Imaging, IEEE Transactions on*, vol. 15, no. 3, pp. 314–326, 1996.

[15] H. Zaidi and I. El Naqa, "PET-guided delineation of radiation therapy treatment volumes: a survey of image segmentation techniques," *European Journal of Nuclear Medicine and Molecular Imaging*, vol. 37, no. 11, pp. 2165–2187, 2010.

[16] L. Massoptier and Y. Song, eds., *Multimodal imaging towards individualized radiotherapy treatments*. TBA, 2014.

[17] I. Wolf, M. Vetter, I. Wegner, M. Nolden, T. Bottger, M. Hastenteufel, M. Schobinger, T. Kunert, and H.-P. Meinzer, "The medical imaging interaction toolkit (MITK): a toolkit facilitating the creation of interactive software by extending VTK and ITK," in *Medical Imaging 2004*, pp. 16–27, International Society for Optics

and Photonics, 2004.

[18] E. Breatnach, G. C. Abbott, and R. G. Fraser, "Dimensions of the normal human trachea," *American Journal of Roentgenology*, vol. 142, no. 5, pp. 903–906, 1984.

[19] W. E. Lorensen and H. E. Cline, "Marching cubes: A high resolution 3D surface construction algorithm," in *ACM Siggraph Computer Graphics*, vol. 21, pp. 163–169, ACM, 1987.

[20] E. W. Dijkstra, "A note on two problems in connexion with graphs," *Numerische Mathematik*, vol. 1, no. 1, pp. 269–271, 1959.

[21] A. S. Glassner, *An introduction to ray tracing.* Morgan Kaufmann, 1989.

[22] D. Marr and E. Hildreth, "Theory of edge detection," *Proceedings of the Royal Society of London. Series B. Biological Sciences*, vol. 207, no. 1167, pp. 187–217, 1980.

[23] T. Fechter, J. Dolz, H. Kirisli, A. Chirindel, S. Adebahr, T. Schimek-Jasch, M. Vermandel, L. Massoptier, and U. Nestle, "Evaluation of an integrated minimally interactive tool for the segmentation of relevant oar in lung cancer," *International Journal of Radiation Oncology* Biology* Physics*, vol. 90, no. 1, p. S817, 2014.

[24] L. Massoptier and Y. Song, eds., *Multimodal imaging towards individualized radiotherapy treatments.* TBA, 2014.

[25] A. Grgic, U. Nestle, A. Schaefer-Schuler, S. Kremp, C.-M. Kirsch, and D. Hellwig, "FDG-PET–based radiotherapy planning in lung cancer: optimum breathing protocol and patient positioning—an intraindividual comparison," *International Journal of Radiation Oncology* Biology* Physics*, vol. 73, no. 1, pp. 103–111, 2009.

[26] M. E. Rodríguez-Ruiz, I. San Miguel, I. Gil-Bazo, J. L. Perez-Gracia, L. Arbea, M. Moreno-Jimenez, and J. Aristu, "Pathological vertebral fracture after stereotactic body radiation therapy for lung metastases. case report and literature review.," *Radiation Oncology*, vol. 7, p. 50, 2012.

Installation manual for the MITK danger zone plugin

The installation of the danger zone plugin comprises 3 steps. The source code of the plugin is split into 3 subfolders. One folder named 'mymitkutils' and 2 plugin folders (org.mitk.homburg and org.mitk.dangerzone). The source code can be asked from the author by mail (tobias.fechter@uniklinik-freiburg.de).

- In the first step MITK has to be compiled with the sources available at the homepage (http://mitk.org/wiki/Downloads). A comprehensive build instruction can be found at http://docs.mitk.org/nightly-qt4/BuildInstructionsPage.html. The plugin was tested against version 2013.09.0, compatibility with other versions can not be guaranteed.

- After the compilation of MITK place the 'mymitkutils' folder in the 'Utilities' folder of the MITK source directory and add 'mymitkutils' to the 'subdirs' section in the file 'CmakeLists.txt'. Then recompile the MITK. The file 'CmakeLists.txt' is also located in the ' Utilities' folder and should look like this:

```
 1 SUPPRESS_ALL_WARNINGS()
 2
 3 # most stuff of these uses itk_zlib.h (via mitkIpPic.h)
 4 find_package(ITK)
 5 include(${ITK_USE_FILE})
 6
 7 # some legacy util files include in the old style with prefixed directory,
 8 # like #include <ipPic/mitkIpPic.h>
 9 include_directories(.)
10
11 subdirs(
12   ipPic
13   ipFunc
14   ipSegmentation
15   mbilog
16   qtsingleapplication
17   KWStyle
18   mymitkutils
19 )
20
21 # mbilog is independent of mitk, and cant use mitk macros
22 # configuring happens through mbilog/mbilogConfig.cmake.in
23 set(mbilog_INCLUDE_DIRS "${CMAKE_CURRENT_SOURCE_DIR}/mbilog"
   "${CMAKE_CURRENT_BINARY_DIR}/mbilog")
24 set(mbilog_CONFIG_FILE "${PROJECT_BINARY_DIR}/${MODULES_CONF_DIRNAME}/
   mbilogConfig.cmake" CACHE INTERNAL "Path to module config" FORCE)
25 configure_file("${CMAKE_CURRENT_SOURCE_DIR}/mbilog/mbilogConfig.cmake.in"
   "${mbilog_CONFIG_FILE}")
```

- In the third step place the two plugin folders in the 'Plugins' directory of the MITK source directory and add the two folder names followed by ':ON' to the 'set(MITK_EXT_PLUGINS' section in the file 'PluginList.cmake'. Then recompile again. After the compilation finished the danger zone plugin is available in the mitkWorkbench. The file 'PluginList.cmake' should look like this:

```
1
2 # Plug-ins must be ordered according to their dependencies
3
4 set(MITK_EXT_PLUGINS
5    org.mitk.core.services:ON
6    org.mitk.gui.common:ON
7    org.mitk.planarfigure:ON
8    org.mitk.gui.qt.application:ON
9    org.mitk.gui.qt.common:ON
10   org.mitk.gui.qt.stdmultiwidgeteditor:ON
11   org.mitk.gui.qt.datamanager:ON
12   org.mitk.gui.qt.datamanagerlight:OFF
13   org.mitk.gui.qt.properties:ON
14   org.mitk.gui.qt.basicimageprocessing:ON
15   org.mitk.gui.qt.dicom:ON
16   org.mitk.gui.qt.imagecropper:ON
17   org.mitk.gui.qt.imagenavigator:ON
18   org.mitk.gui.qt.materialeditor:OFF
19   org.mitk.gui.qt.measurementtoolbox:ON
20   org.mitk.gui.qt.pointsetinteraction:ON
21   org.mitk.gui.qt.python:OFF
22   org.mitk.gui.qt.registration:ON
23   org.mitk.gui.qt.remeshing:ON
24   org.mitk.gui.qt.segmentation:ON
25   org.mitk.gui.qt.simulation:ON
26   org.mitk.gui.qt.toftutorial:OFF
27   org.mitk.gui.qt.tofutil:OFF
28   org.mitk.gui.qt.ugvisualization:OFF
29   org.mitk.gui.qt.ultrasound:OFF
30   org.mitk.gui.qt.volumevisualization:ON
31   org.mitk.homburg:ON
32   org.mitk.dangerzone:ON
33   )
```

If you have further questions regarding the installation process or the usage of the plugin, please don't hesitate to contact the first author.